Determination of the pion form factor up to $Q^2 = 4$ GeV^2 from single-charged-pion electroproduction

C. J. Bebek, C. N. Brown,* M. Herzlinger, S. D. Holmes, C. A. Lichtenstein,‡ F. M. Pipkin, S. Raither, and L. K. Sisterson§

Cyclotron Laboratory, Harvard University, Cambridge, Massachusetts 02138

(Received 3 December 1974; revised manuscript received 22 September 1975)

We report new measurements of the electroproduction of single charged pions from both hydrogen and deuterium targets carried out at the Wilson Synchrotron Laboratory at Cornell University. Measurements were made at the (W, Q^2) points (2.15 GeV, 1.2 GeV^2), (2.15, 4.0), and (3.11, 1.2) with hydrogen and deuterium and at (2.15, 2.0), (2.67, 3.4), and (3.11, 1.7) with only hydrogen. The deuterium data were used to determine the ratio of the cross sections for the reactions $\gamma_V d \to \pi^+ n n_s$ and $\gamma_V d \to \pi^- p p_s$ and thus to measure the isoscalar contribution to the reaction $\gamma_V p \to \pi^+ n$. The data are consistent with the hypothesis that this ratio is a universal function of the momentum transfer. The measured ratio was used to determine from the hydrogen data and the data taken in earlier experiments the isovector component of the cross section. The dispersion theory formulated by Berends was then used to determine from the isovector component the pion form factor in the Q^2 range from 0.2 to 4.0 GeV^2. A simple pole expression of the form $[1 + Q^2/(0.471 \pm 0.010)]^{-1}$ gives a good fit to the data.

I. INTRODUCTION

Both the vector-dominance model (VDM) and dispersion theory (DT) have been used to construct models for the photoproduction reaction

$$\gamma + p \to \pi^+ + n \tag{1}$$

and for the electroproduction reaction

$$e^- + p \to e^- + \pi^+ + n\,. \tag{2}$$

The dispersion theory models have been more successful in describing both photoproduction and electroproduction experiments.[1] Briefly the DT model assumes that (1) the amplitude is real at high energies and thus the imaginary part is given by low-energy data; (2) the imaginary part is dominated by the $\Delta(1236)$; (3) this resonance is excited mainly by the M_{1+}[3] multipole; (4) the real part at high energies is given by a dispersion integral over the imaginary amplitude with the generalized Born approximation giving the pole terms which include s- and u-channel nucleon poles and the important t-channel pion pole. This model predicts that the pion pole dominates the cross section near 0°. The analysis implicitly assumes that the pion electroproduction amplitude is purely isovector. This is true for the $\Delta(1236)$, an isospin $\frac{3}{2}$ particle, and by G parity for the pion pole. Within the framework of these assumptions, measurements of single-pion electroproduction give a precise determination of the pion form factor. Figure 1 shows how the forward cross section for reaction (2) depends on the total center-of-mass energy, W, and the photon mass, Q^2, with two popular expressions for the pion form factor.[2] It also shows the transverse component of the cross section due to the s- and u-channel poles. As one goes to higher Q^2 and higher W the scalar pion pole term becomes increasingly dominant.

This report summarizes the results of further measurements of the electroproduction of single charged pions carried out at the Wilson Synchrotron Laboratory at Cornell University. Measurements with a deuterium target yielded cross sections for reaction (2) and for the reaction

$$e^- + n \to e^- + \pi^- + p\,. \tag{3}$$

The ratio was used to determine the isoscalar component of the cross section and to determine from the hydrogen data the isovector electroproduction cross section. Berends's theory[2] was then used to determine the pion form factor up to $Q^2 = 4$ GeV^2. These measurements represent a continuation of similar measurements at lower energies by some members of the group. Hence we will rely on previous reports[1,3] to supply the background material for the kinematics, experimental techniques, and analysis procedures used to determine the pion form factor from the data.[4-7]

II. EXPERIMENT

Figure 2 shows a schematic diagram of the apparatus. The apparatus was essentially the same as that used in the previously reported work carried out at Cornell.[3] The heavy liquid shower counter used on the electron arm in the earlier experiment was replaced with a lead-lucite sandwich counter. The trigger counters on the electron arm were replaced by a larger set of count-

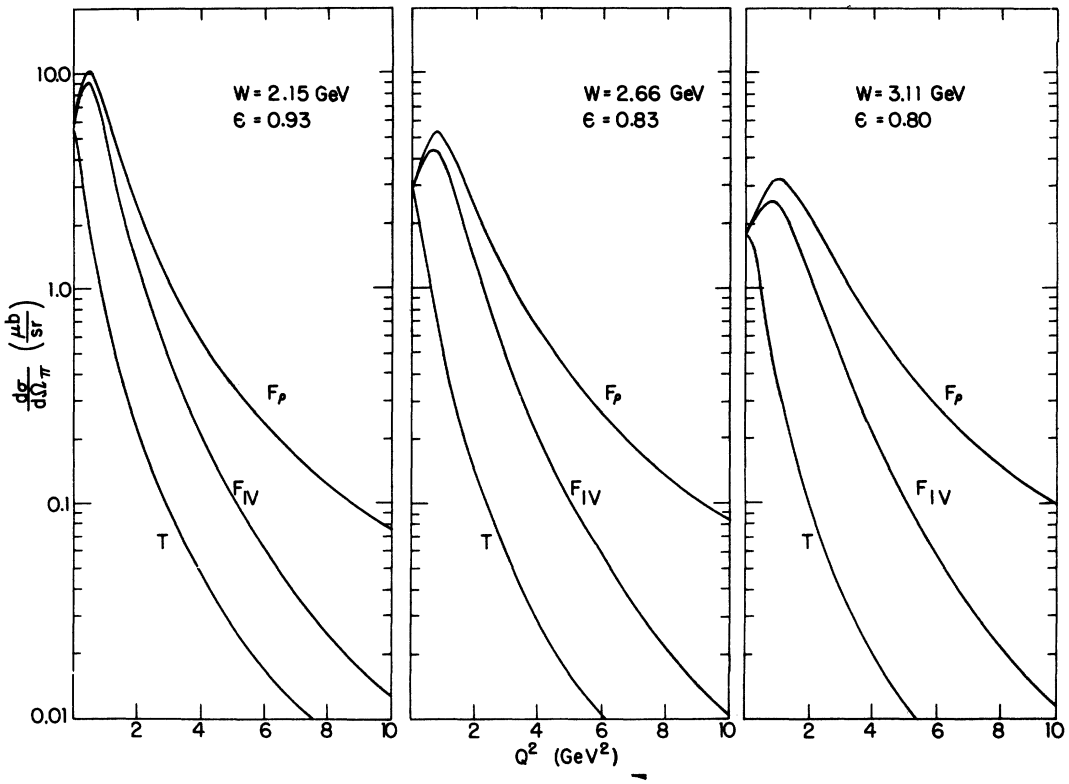

FIG. 1. A plot showing the behavior versus Q^2 of the 0° single-pion electroproduction cross section for the three center-of-mass energies W used in this experiment. The curves denoted by F_ρ and F_{1V} give the cross section for two popular forms for the pion form factor. The curve denoted by T gives the total contribution to the cross section due to the transverse term including the dispersion theory corrections. The rest of the cross section is due to the one-pion-exchange diagram.

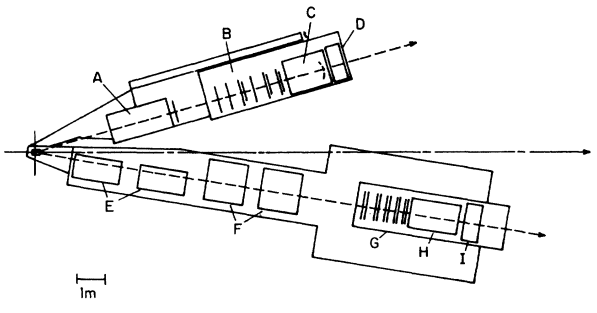

FIG. 2. A schematic diagram of the apparatus: A, 20D84 bending magnet; B, wire-chamber planes and scintillation counters; C, Freon Čerenkov counter; D, lead-Lucite shower counter; E, 8Q48 half quadrupole magnets; F, 18D36 bending magnets; G, proportional wire chambers and scintillation counters; H, freon Čerenkov counter; I, lead-Lucite shower counter.

ers that increased the momentum acceptance from 30% to 50% full width at half maximum (FWHM). A seventh spark chamber was placed just behind the bending magnet on the hadron arm. This increased the momentum resolution. The increase in the acceptance of the electron arm and in the available energy of the accelerator from 10 to 12 GeV enabled us to reach higher energies and momentum transfers than in the earlier experiment.

Figure 3 shows the virtual-photon energy, ν, and the virtual-photon mass squared, $-Q^2$, for the points at which data were taken. The hadron spectrometer was always set along the direction of the virtual photon so as to detect pions produced near 0° in the virtual-photon–target-nucleon center-of-mass system. Data were taken with a deuterium target at data points 8, 9, and 13.

Figure 4 shows typical missing mass spectra for both hydrogen and deuterium targets. There is a clear missing mass peak due to single-pion

electroproduction for both targets. The deuteron structure gives rise to a broadening of the missing mass peak. The difference in the positions of the missing mass peaks for hydrogen and deuterium indicates the reproducibility of the apparatus. These particular hydrogen measurements were the first data point; these deuterium measurements were the last data point. The apparatus was moved and resurveyed several times in between and the calibration determined during the initial hydrogen measurements was used in analyzing the deuterium data. In the final analysis all events within the cuts shown were constrained by adjusting the scattered electron and pion momenta equally to give the known nucleon mass. No correction was made to the deuterium data for events kinematically excluded by the data-analysis procedure because of Fermi motion of the target nucleons. A Monte Carlo calculation based on the Hulthén[8] wave function for the deuteron indicated that the loss was less than 0.5%. The events were then binned in the variables, θ, the polar angle of the emitted pion in the center-of-mass system of the virtual-photoproduction reaction, and ϕ, the angle between the plane determined by the virtual-photoproduction reaction and the electron-scattering plane. The bins had a typical full width at half maximum of 0.12 GeV in W, 0.12 GeV^2 in Q^2, and 0.02 in ϵ.

A Monte Carlo calculation assuming unit center-of-mass cross section and incorporating multiple scattering, detector resolution, and geometrical effects was used to determine the acceptance. The normalization of the experiment was checked by independently observing elastically scattered electrons in both spectrometers and comparing the observed cross sections with the measured elastic-scattering cross section. The Monte Carlo program gave an angular resolution of about 0.3° full width in the center-of-mass system and indicated that the resolution in angle and energy was multiple-scattering dominated.

The measured cross sections were corrected for nuclear absorption [(6.8 ± 2)%], dead time

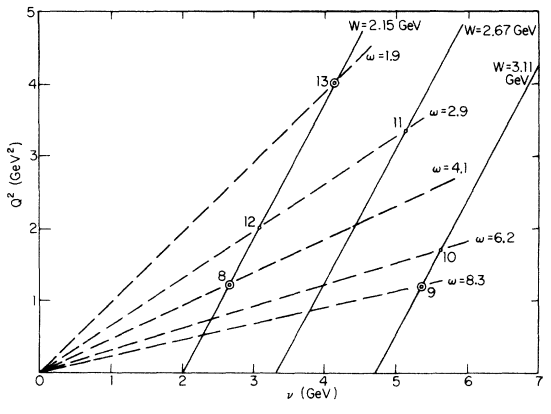

FIG. 3. A diagram showing the nominal values of Q^2 and W at which data were taken. The single circles indicate points at which data were taken with a hydrogen target only; the double circles indicate points at which data were taken with both dydrogen and deuterium targets.

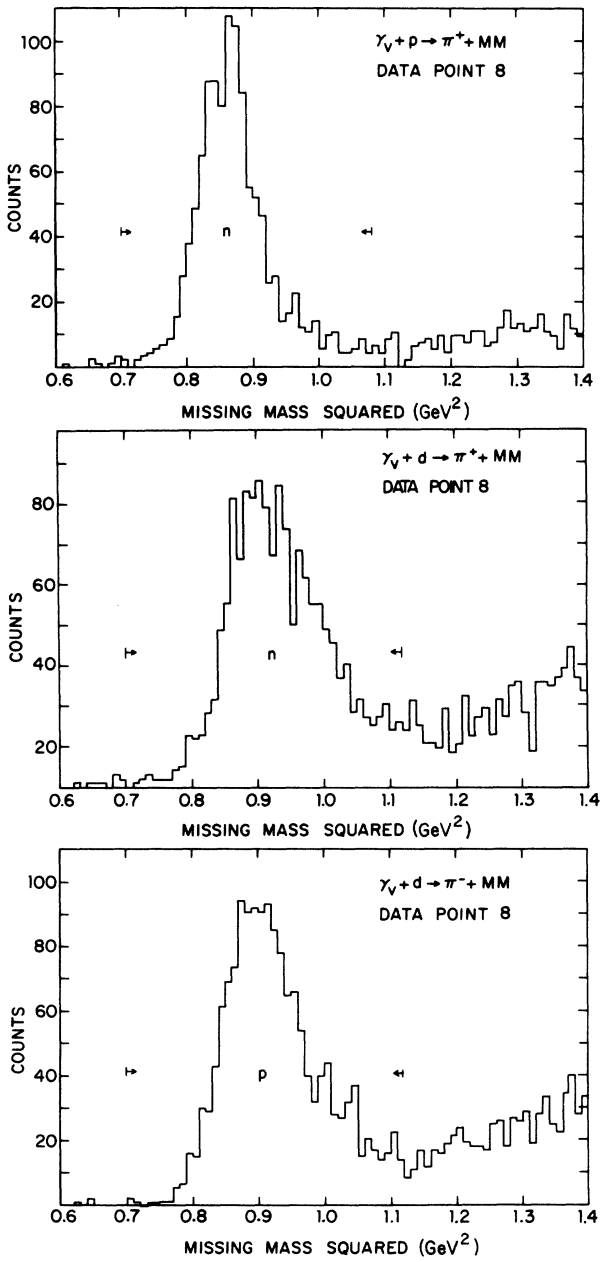

FIG. 4. Missing mass squared spectra for hydrogen and deuterium targets at the data point with nominal settings $W = 2.15$ GeV and $Q^2 = 1.2$ GeV^2.

[(5±2)%], target wall background [(5±2)%], and pion decay [(3±1)%]. The sum of all corrections was less than 20% at all data points.

The cross sections were also corrected for losses due to the radiation of soft photons. The prescription for the radiative correction was taken from the work of Bartl and Urban.[9] It was checked by an independent calculation based on the work of Meister and Yennie.[10] The two calculations agreed to better than 0.5% for the data presented here. The radiative correction was roughly 40% for all the data points.

The errors on the cross sections presented in this paper are statistical only. There is an additional systematic uncertainty which is estimated to be less than 7%. This systematic uncertainty is based on the normalization check with the electron-scattering measurements and the uncertainty in the corrections to the data.

III. RESULTS

Tables I(a) through I(f) list the $\pi^+ n$ cross sections for a hydrogen target determined in this experiment. Tables II(a) and II(b) list the π^+ cross sections for two of the deuterium points. Table III summarizes the ratio of the π^- and π^+ cross sections for the deuterium measurements. Owing to the high correlation of the average virtual-photon parameters with the observed angle between the pion and the virtual-photon direction, the average values of the virtual-photon parameters over the events in a bin are also included for each bin.

Figures 5 through 8 show the $\pi^+ n$ cross sections for a hydrogen target as a function of the polar angle θ of the emitted pion for the virtual-photoproduction plane parallel to the electron-scattering plane ($\phi = 0°$ or 180°) and for the virtual-photoproduction plane perpendicular to the electron-scattering plane ($\phi = -90°$ or 90°). The values of W, Q^2, and ϵ listed for each curve are the average values for the central bin. The values of W, Q^2, and ϵ change considerably as θ changes, and this change must be taken into account if the data are compared with theory or used to determine the interference terms.

Figure 5 also shows the data taken in the earlier experiment at Cornell[3] for $W = 2.15$ GeV, $Q^2 = 1.2$ GeV^2. The agreement between the two experiments is good.

Figures 6(e), 6(f), 7(c), and 7(d) show a comparison between the π^+ data taken with a hydrogen target and the π^+ data taken with a deuterium target. The two cross sections are in excellent agreement and give no indication of a suppression of the deuterium cross sections in the forward direction as is observed in photoproduction.[11-19] A similar result was obtained in earlier measurements at the Cambridge Electron Accelerator.[20]

Figures 9 through 12 show the ratio

$$R = \frac{(d\sigma/d\Omega_\pi)(e^- + D \to e^- + \pi^- + p + p_s)}{(d\sigma/d\Omega_\pi)(e^- + D \to e^- + \pi^+ + n + n_s)} \tag{4}$$

for two of the points at which deuterium data were taken. Here the subscript s denotes the spectator particle. Photoproduction data suggest that in this domain R is a universal function of momentum transfer of the form

$$1 - A\sqrt{-t}\,, \tag{5}$$

and that it is not a strong function of energy.[11,12,21,22,23] Figure 13 shows a plot of R versus the momentum transfer t for the data taken in this experiment and for the earlier CEA data together with the fit. The least-squares determined value for A is

$$A = 0.817 \pm 0.058\,.$$

The χ^2 is 38.6 for 49 degrees of freedom. Figure 14 shows R for photoproduction measurements together with the fit to the electroproduction data. R is somewhat larger for electroproduction than for photoproduction.

In terms of the isovector and isoscalar virtual-photoproduction amplitudes, R can be written

$$R = \frac{|A_V|^2 + |A_S|^2 - 2\,\mathrm{Re}(A_S^* A_V)}{|A_V|^2 + |A_S|^2 + 2\,\mathrm{Re}(A_S^* A_V)}$$

$$= 1 - 4\frac{\mathrm{Re}(A_S^* A_V)}{|A_V|^2 + |A_S|^2 + 2\,\mathrm{Re}(A_S^* A_V)}\,.$$

IV. DETERMINATION OF PION FORM FACTOR

In order to use Berends's theory to determine the pion form factor it is necessary to determine the isovector component of the virtual-photoproduction cross section. To do this we first determine the cross section for pions produced at center-of-mass angles less than 3° (the central bin). We then use R as given by the fit at the average t for the data and determine the isovector component by multiplying the measured cross section by $[(\frac{1}{2}(1+R)]$. To be precise this gives

$$\tfrac{1}{2}(1+R)\frac{d\sigma}{d\Omega}(\gamma p \to \pi^+ n) = |A_V|^2 + |A_S|^2\,.$$

To obtain a better estimate of the isovector component it is necessary to have information on the relative phase of the isoscalar and isovector amplitudes. If we assume that they are both real or have the same phase, the error in the calculated isovector component of the cross section for the data point with the smallest value for R ($R = 0.436$)

TABLE I. The bins and the center-of-mass virtual-photoproduction cross sections for the reaction $\gamma_V + p \to \pi^+ + n$ derived from measurements with a hydrogen target. The uncertainties are statistical only. N is the number of events in the bin.

Bin			Kinematic averages							Result
ϕ (deg)	θ (deg)	θ (deg)	W (GeV)	Q^2 (GeV^2)	ϵ	$\epsilon\cos2\phi$	$[\epsilon(\epsilon+1)/2]^{1/2}\cos\phi$	$-t$ (GeV^2)	N	$(d\sigma/d\Omega_\pi)$ (μb/sr)
					(a) Data point 8 (H_2)					
all	0→3	1.803	2.143	1.216	0.947	0.008	−0.036	0.069	64	5.080 ±0.740
−45→45	3→6	4.784	2.064	1.211	0.954	0.554	0.854	0.086	41	3.561 ±0.623
	6→9	7.807	2.017	1.256	0.956	0.613	0.872	0.108	59	3.373 ±0.500
	9→12	10.475	1.980	1.263	0.959	0.663	0.888	0.128	73	3.657 ±0.481
	12→15	13.605	1.936	1.269	0.962	0.672	0.891	0.157	74	3.359 ±0.443
	15→18	16.460	1.893	1.285	0.964	0.719	0.906	0.190	37	1.632 ±0.295
	18→21	19.302	1.845	1.296	0.966	0.804	0.931	0.224	34	1.852 ±0.338
	21→24	22.354	1.809	1.323	0.968	0.815	0.935	0.267	24	1.446 ±0.348
	24→27	25.094	1.763	1.327	0.970	0.852	0.947	0.303	20	1.643 ±0.416
	27→30	28.435	1.708	1.314	0.973	0.878	0.955	0.347	31	3.363 ±0.763
	30→33	31.390	1.675	1.361	0.973	0.880	0.956	0.404	15	2.703 ±0.755
	33→36	34.273	1.650	1.352	0.975	0.837	0.945	0.443	11	3.890 ±1.306
45→135	3→6	4.937	2.141	1.207	0.947	−0.604	−0.090	0.076	57	4.659 ±0.713
	6→9	7.626	2.157	1.219	0.946	−0.595	−0.068	0.087	75	3.743 ±0.488
	9→12	10.584	2.145	1.213	0.947	−0.616	0.037	0.105	78	3.148 ±0.401
	12→15	13.535	2.200	1.196	0.942	−0.507	−0.174	0.123	60	3.068 ±0.497
	15→18	16.443	2.255	1.173	0.937	−0.619	−0.270	0.151	24	1.365 ±0.309
	18→21	19.260	2.342	1.145	0.928	−0.439	−0.499	0.187	14	1.682 ±0.475
135→225	3→6	4.462	2.216	1.188	0.941	0.720	−0.895	0.065	37	4.429 ±0.837
	6→9	7.538	2.261	1.184	0.967	0.582	−0.853	0.074	42	2.695 ±0.469
	9→12	10.465	2.309	1.147	0.932	0.585	−0.852	0.087	50	2.380 ±0.364
	12→15	13.537	2.362	1.139	0.926	0.559	−0.842	0.113	54	2.304 ±0.337
	15→18	16.162	2.415	1.133	0.919	0.537	−0.831	0.144	25	0.917 ±0.200
	18→21	19.508	2.485	1.078	0.912	0.622	−0.853	0.195	24	0.887 ±0.198
	21→24	22.481	2.535	1.081	0.904	0.631	−0.851	0.254	10	0.338 ±0.108
	24→27	25.425	2.586	1.051	0.896	0.578	−0.832	0.323	7	0.245 ±0.094
	27→30	28.558	2.658	1.009	0.886	0.538	−0.816	0.414	13	0.450 ±0.125
−135→−45	3→6	4.353	2.144	1.215	0.947	−0.681	−0.156	0.074	23	3.060 ±0.706
	6→9	7.656	2.137	1.191	0.948	−0.488	0.042	0.085	18	3.125 ±0.814
					(b) Data point 9 (H_2)					
all	0→3	1.975	3.082	1.198	0.825	0.029	0.139	0.019	135	3.091 ±0.309
−45→45	3→6	4.606	2.965	1.275	0.849	0.594	0.814	0.035	132	3.070 ±0.316
	6→9	7.464	2.895	1.304	0.862	0.598	0.821	0.058	157	2.418 ±0.217
	9→12	10.492	2.817	1.344	0.876	0.590	0.826	0.093	131	1.600 ±0.155
	12→15	13.512	2.741	1.396	0.888	0.651	0.849	0.135	135	1.487 ±0.138
	15→18	16.477	2.671	1.429	0.898	0.677	0.862	0.182	88	0.860 ±0.099
	18→21	19.201	2.603	1.464	0.906	0.713	0.876	0.230	63	0.649 ±0.091
	21→24	22.319	2.510	1.493	0.918	0.838	0.917	0.287	48	0.584 ±0.096
	24→27	25.376	2.444	1.551	0.924	0.864	0.928	0.350	21	0.345 ±0.081
	27→30	28.391	2.365	1.569	0.932	0.891	0.938	0.409	16	0.371 ±0.097
45→135	3→6	4.603	3.087	1.201	0.823	−0.511	0.002	0.031	129	2.490 ±0.249
	6→9	7.578	3.090	1.211	0.821	−0.513	0.029	0.057	147	1.926 ±0.173
	9→12	10.449	3.080	1.209	0.823	−0.579	0.056	0.092	142	1.365 ±0.124
	12→15	13.361	3.094	1.207	0.818	−0.547	0.051	0.142	121	1.016 ±0.100
	15→18	16.202	3.124	1.197	0.810	−0.534	0.031	0.203	53	0.508 ±0.074
	18→21	18.986	3.174	1.168	0.794	−0.449	0.005	0.279	22	0.416 ±0.142
135→225	3→6	4.437	3.211	1.139	0.793	0.474	−0.750	0.028	50	1.996 ±0.310
	6→9	7.419	3.281	1.087	0.774	0.412	−0.721	0.054	39	1.256 ±0.213
	9→12	10.315	3.365	1.037	0.749	0.413	−0.710	0.096	28	0.695 ±0.177
	12→15	13.656	3.484	0.976	0.707	0.149	−0.604	0.170	10	0.415 ±0.132
−135→−45	3→6	4.276	3.062	1.213	0.830	−0.490	0.117	0.030	28	2.361 ±0.499
	6→9	7.282	2.949	1.251	0.854	−0.295	0.502	0.055	11	3.072 ±1.069

TABLE I. *(Continued)*

Bin ϕ (deg)	ϕ (deg)	θ (deg)	W (GeV)	Q^2 (GeV^2)	ϵ	$\epsilon\cos2\phi$	$[\epsilon(\epsilon+1)/2]^{1/2}\cos\phi$	$-t$ (GeV^2)	N	Result $(d\sigma/d\Omega_\pi)$(μb/sr)
				(c) Data point 10 (H_2)						
all	0→3	1.919	3.093	1.712	0.794	−0.028	0.049	0.034	84	2.519 ± 0.325
−45→45	3→6	4.600	2.983	1.811	0.819	0.569	0.791	0.054	63	1.959 ± 0.305
	6→9	7.525	2.914	1.869	0.833	0.580	0.801	0.083	82	1.549 ± 0.214
	9→12	10.607	2.845	1.913	0.846	0.594	0.812	0.124	103	1.572 ± 0.174
	12→15	13.617	2.782	1.956	0.857	0.537	0.800	0.172	80	0.932 ± 0.121
	15→18	16.481	2.701	2.020	0.870	0.632	0.835	0.228	58	0.656 ± 0.090
	18→21	19.530	2.647	2.088	0.877	0.668	0.849	0.294	47	0.436 ± 0.081
	21→24	22.443	2.565	2.125	0.888	0.745	0.877	0.361	31	0.362 ± 0.067
	24→27	25.234	2.490	2.158	0.899	0.816	0.902	0.427	23	0.240 ± 0.080
	27→30	28.331	2.433	2.191	0.906	0.842	0.912	0.505	19	0.320 ± 0.075
	30→33	31.312	2.362	2.247	0.912	0.859	0.920	0.592	12	0.222 ± 0.074
45→135	3→6	4.598	3.090	1.718	0.794	−0.516	0.077	0.048	75	1.748 ± 0.243
	6→9	7.467	3.118	1.698	0.787	−0.509	−0.047	0.072	99	1.576 ± 0.187
	9→12	10.280	3.099	1.725	0.780	−0.477	0.045	0.111	102	1.087 ± 0.134
	12→15	13.415	3.077	1.725	0.795	−0.497	0.078	0.165	86	0.732 ± 0.088
	15→18	16.486	3.091	1.721	0.790	−0.471	0.076	0.234	57	0.530 ± 0.076
	18→21	19.368	3.113	1.704	0.782	−0.505	0.064	0.313	31	0.586 ± 0.099
135→225	3→6	4.389	3.197	1.632	0.768	0.555	−0.762	0.041	21	1.146 ± 0.273
	6→9	7.672	3.283	1.568	0.743	0.378	−0.695	0.069	28	1.358 ± 0.282
	9→12	10.457	3.349	1.526	0.724	0.317	−0.666	0.111	22	1.010 ± 0.232
				(d) Data point 11 (H_2)						
all	0→3	1.670	2.658	3.301	0.825	0.004	0.021	0.162	25	0.770 ± 0.174
−45→45	3→6	4.532	2.567	3.432	0.837	0.551	0.793	0.202	16	0.589 ± 0.162
	6→9	7.412	2.525	3.481	0.843	0.599	0.812	0.241	19	0.531 ± 0.133
	9→12	10.768	2.451	3.556	0.853	0.519	0.793	0.311	34	0.738 ± 0.152
	12→15	13.342	2.419	3.593	0.857	0.555	0.807	0.358	24	0.434 ± 0.096
	15→18	16.537	2.344	3.661	0.866	0.532	0.803	0.444	29	0.494 ± 0.100
	18→21	19.264	2.295	3.732	0.871	0.616	0.831	0.522	27	0.441 ± 0.091
	21→24	22.705	2.242	3.758	0.877	0.649	0.844	0.618	20	0.369 ± 0.087
	24→27	25.768	2.150	3.830	0.887	0.825	0.898	0.745	13	0.276 ± 0.081
	27→30	28.536	2.126	3.897	0.888	0.819	0.898	0.839	11	0.252 ± 0.079
45→135	3→6	4.926	2.668	3.296	0.821	−0.527	−0.123	0.172	25	1.206 ± 0.290
	6→9	7.639	2.667	3.308	0.821	−0.462	−0.022	0.200	35	0.689 ± 0.130
	9→12	10.537	2.638	3.353	0.825	−0.513	0.045	0.246	32	0.541 ± 0.112
	12→15	13.536	2.685	3.269	0.818	−0.462	−0.022	0.281	30	0.431 ± 0.085
	15→18	16.310	2.703	3.256	0.814	−0.539	−0.071	0.336	37	0.508 ± 0.097
	18→21	19.518	2.737	3.268	0.806	−0.422	−0.114	0.417	13	0.196 ± 0.055
135→225	3→6	4.765	2.750	3.241	0.808	0.546	−0.779	0.150	16	0.572 ± 0.158
	6→9	6.985	2.802	3.154	0.798	0.512	−0.765	0.159	26	0.809 ± 0.181
	9→12	10.892	2.889	3.001	0.784	0.419	−0.729	0.188	8	0.198 ± 0.072
	12→15	13.392	2.925	3.016	0.773	0.440	−0.730	0.234	15	0.286 ± 0.108
	15→18	16.162	3.002	2.932	0.755	0.551	−0.756	0.290	11	0.261 ± 0.081
				(e) Data point 12 (H_2)						
all	0→3	1.998	2.140	1.988	0.942	−0.058	0.015	0.157	84	2.281 ± 0.289
−45→45	3→6	4.761	2.071	2.027	0.947	0.596	0.862	0.193	58	2.053 ± 0.313
	6→9	7.674	2.026	2.023	0.950	0.607	0.867	0.219	87	1.860 ± 0.228
	9→12	10.481	1.985	2.053	0.952	0.669	0.886	0.253	91	1.653 ± 0.194
	12→15	13.285	1.948	2.072	0.954	0.648	0.881	0.291	69	1.030 ± 0.132
	15→18	16.381	1.910	2.095	0.956	0.592	0.866	0.340	73	1.118 ± 0.140

TABLE I. *(Continued)*

Bin			Kinematic averages							Result
ϕ (deg)	θ (deg)	θ (deg)	W (GeV)	Q^2 (GeV^2)	ϵ	$\epsilon\cos2\phi$	$[\epsilon(\epsilon+1)/2]^{1/2}\cos\phi$	$-t$ (GeV^2)	N	$(d\sigma/d\Omega_\pi)$(μb/sr)
					(e) Data point 12 (H_2)					
−45→45	18→21	19.368	1.857	2.119	0.959	0.753	0.913	0.400	70	1.148 ± 0.147
	21→24	22.481	1.805	2.135	0.961	0.834	0.937	0.461	63	1.216 ± 0.169
	24→27	25.477	1.762	2.158	0.963	0.809	0.931	0.529	57	1.202 ± 0.179
	27→30	28.408	1.715	2.167	0.965	0.867	0.948	0.596	37	1.168 ± 0.204
	30→33	31.447	1.681	2.182	0.966	0.844	0.943	0.665	31	1.072 ± 0.213
	33→36	34.546	1.643	2.213	0.967	0.813	0.935	0.742	17	1.061 ± 0.272
45→135	3→6	4.708	2.151	2.009	0.941	−0.639	−0.049	0.167	52	1.366 ± 0.213
	6→9	7.402	2.148	1.992	0.941	−0.571	−0.031	0.180	93	1.591 ± 0.182
	9→12	10.402	2.159	1.983	0.940	−0.632	−0.072	0.195	114	1.747 ± 0.186
	12→15	13.494	2.170	1.962	0.940	−0.582	−0.087	0.222	102	1.444 ± 0.158
	15→18	16.288	2.211	1.958	0.936	−0.608	−0.165	0.248	59	0.943 ± 0.134
	18→21	19.443	2.248	1.947	0.932	−0.396	−0.214	0.293	46	1.005 ± 0.158
	21→24	22.307	2.374	1.845	0.923	−0.418	−0.471	0.318	20	0.959 ± 0.227
135→225	3→6	4.836	2.221	1.936	0.936	0.604	−0.860	0.141	29	1.159 ± 0.257
	6→9	7.541	2.267	1.937	0.932	0.646	−0.869	0.146	95	2.078 ± 0.242
	9→12	10.579	2.308	1.907	0.929	0.555	−0.842	0.161	87	1.469 ± 0.176
	12→15	13.528	2.363	1.877	0.924	0.550	−0.838	0.183	73	1.081 ± 0.139
	15→18	16.541	2.415	1.844	0.918	0.589	−0.847	0.217	64	0.797 ± 0.105
	18→21	19.174	2.459	1.831	0.913	0.543	−0.830	0.259	51	0.566 ± 0.084
	21→24	22.195	2.516	1.811	0.906	0.561	−0.832	0.319	37	0.401 ± 0.071
	24→27	25.820	2.585	1.749	0.899	0.631	−0.850	0.407	21	0.234 ± 0.056
	27→30	28.304	2.635	1.699	0.893	0.505	−0.810	0.479	18	0.262 ± 0.063
−135→−45	3→6	4.605	2.130	2.012	0.942	−0.582	0.057	0.173	39	2.104 ± 0.384
	6→9	7.511	2.147	1.981	0.942	−0.546	0.028	0.177	35	1.530 ± 0.295
	9→12	10.293	2.087	2.003	0.946	−0.488	0.320	0.213	21	1.287 ± 0.304
	12→15	13.316	2.018	2.040	0.950	−0.361	0.508	0.261	13	1.996 ± 0.626
					(f) Data point 13 (H_2)					
all	0→3	1.901	2.139	3.991	0.883	−0.020	0.218	0.447	16	0.513 ± 0.156
−45→45	3→6	4.726	2.081	3.975	0.890	0.600	0.836	0.519	5	0.182 ± 0.084
	6→9	7.329	2.020	4.075	0.894	0.584	0.832	0.581	18	0.430 ± 0.120
	9→12	10.672	2.002	4.086	0.896	0.427	0.788	0.611	19	0.307 ± 0.075
	12→15	13.295	1.930	4.140	0.902	0.685	0.866	0.727	30	0.550 ± 0.112
	15→18	16.535	1.882	4.234	0.904	0.504	0.814	0.844	15	0.250 ± 0.068
	18→21	19.520	1.839	4.270	0.907	0.687	0.870	0.955	10	0.218 ± 0.073
	21→24	22.452	1.796	4.238	0.911	0.671	0.867	1.037	20	0.338 ± 0.080
	24→27	25.323	1.759	4.299	0.913	0.636	0.858	1.151	17	0.465 ± 0.123
	27→30	28.765	1.685	4.420	0.915	0.787	0.902	1.372	16	0.464 ± 0.126
	30→33	31.181	1.669	4.369	0.918	0.756	0.895	1.405	15	0.589 ± 0.167
45→135	3→6	4.678	2.174	3.932	0.881	−0.543	−0.113	0.423	12	0.370 ± 0.124
	6→9	7.493	2.169	3.961	0.881	−0.568	−0.124	0.457	31	0.678 ± 0.140
	9→12	10.182	2.156	3.989	0.881	−0.618	−0.034	0.485	22	0.308 ± 0.070
	12→15	13.315	2.145	4.021	0.881	−0.609	0.045	0.554	35	0.432 ± 0.081
	15→18	16.705	2.226	3.899	0.874	−0.520	−0.210	0.542	38	0.502 ± 0.091
	18→21	19.125	2.262	3.909	0.869	−0.414	−0.256	0.599	13	0.226 ± 0.065
135→225	3→6	4.893	2.216	3.880	0.877	0.543	−0.810	0.388	9	0.511 ± 0.190
	6→9	7.273	2.259	3.870	0.872	0.537	−0.808	0.391	19	0.477 ± 0.122
	9→12	10.719	2.303	3.855	0.866	0.533	−0.804	0.407	23	0.554 ± 0.130
	12→15	13.333	2.371	3.752	0.859	0.532	−0.801	0.401	31	0.452 ± 0.089
	15→18	16.674	2.440	3.742	0.849	0.517	−0.791	0.436	19	0.304 ± 0.075
	18→21	19.170	2.474	3.673	0.845	0.553	−0.800	0.470	18	0.246 ± 0.061
	21→24	22.362	2.542	3.558	0.837	0.560	−0.798	0.535	21	0.245 ± 0.056
	24→27	25.504	2.578	3.554	0.830	0.434	−0.757	0.627	19	0.224 ± 0.055

TABLE II. The bins and center-of-mass virtual-photoproduction cross sections for the reaction $\gamma_V + p \to \pi^+ + n$ derived from measurements with a deuterium target. The uncertainties are statistical only. N is the number of events in the bin.

Bin					Kinematic averages					Result
ϕ (deg)	θ (deg)	θ (deg)	W (GeV)	Q^2 (GeV^2)	ϵ	$\epsilon\cos2\phi$	$[\epsilon(\epsilon+1)/2]^{1/2}\cos\phi$	$-t$ (GeV^2)	N	$(d\sigma/d\Omega_\pi)$(μb/sr)
					(a) Data point 8 (D_2)					
all	0→3	1.840	2.138	1.212	0.948	0.038	0.049	0.073	76	5.242±0.700
−45→45	3→6	4.677	2.065	1.226	0.953	0.569	0.858	0.090	56	4.466±0.683
	6→9	7.583	2.022	1.234	0.956	0.607	0.871	0.110	87	4.662±0.574
	9→12	10.538	1.980	1.254	0.959	0.649	0.884	0.135	64	2.893±0.421
	12→15	13.225	1.942	1.275	0.961	0.672	0.891	0.161	48	1.978±0.322
	15→18	16.352	1.892	1.270	0.964	0.704	0.902	0.191	53	2.017±0.295
	18→21	19.391	1.852	1.307	0.966	0.766	0.921	0.234	44	1.940±0.331
	21→24	22.399	1.799	1.306	0.969	0.838	0.943	0.274	32	1.713±0.334
	24→27	25.414	1.746	1.308	0.971	0.846	0.946	0.315	19	1.175±0.302
	27→30	28.650	1.708	1.330	0.973	0.890	0.958	0.364	18	1.288±0.535
	30→33	31.424	1.669	1.352	0.974	0.853	0.949	0.404	16	1.977±0.691
45→135	3→6	4.566	2.143	1.200	0.947	−0.562	−0.042	0.078	58	3.590±0.526
	6→9	7.334	2.151	1.210	0.946	−0.614	−0.024	0.090	76	3.376±0.429
	9→12	10.519	2.159	1.190	0.946	−0.531	−0.071	0.107	74	2.741±0.347
	12→15	13.376	2.183	1.188	0.943	−0.617	−0.110	0.128	60	2.312±0.320
	15→18	16.135	2.211	1.175	0.941	−0.599	−0.148	0.153	33	1.668±0.306
	18→21	19.044	2.325	1.164	0.929	−0.378	−0.410	0.192	12	1.249±0.423
135→225	3→6	4.614	2.207	1.165	0.942	0.630	−0.870	0.066	47	3.569±0.597
	6→9	7.526	2.256	1.151	0.938	0.568	−0.850	0.073	59	3.058±0.498
	9→12	10.574	2.312	1.146	0.932	0.578	−0.850	0.090	64	2.603±0.388
	12→15	13.361	2.363	1.120	0.927	0.579	−0.848	0.113	56	2.298±0.329
	15→18	16.339	2.415	1.108	0.920	0.543	−0.834	0.147	32	1.147±0.210
	18→21	19.620	2.471	1.082	0.913	0.518	−0.824	0.197	31	1.036±0.193
	21→24	22.530	2.553	1.041	0.903	0.631	−0.851	0.255	19	0.505±0.166
−135→−45	3→6	4.626	2.145	1.211	0.947	−0.662	0.017	0.076	27	3.518±0.754
	6→9	7.455	2.107	1.194	0.951	−0.483	0.200	0.090	42	5.443±1.004
	9→12	10.323	2.104	1.210	0.950	−0.412	0.198	0.110	16	2.958±1.178
					(b) Data point 9 (D_2)					
all	0→3	1.982	3.063	1.187	0.826	0.095	0.154	0.020	69	2.804±0.383
−45→45	3→6	4.472	2.959	1.254	0.849	0.569	0.806	0.034	59	2.727±0.403
	6→9	7.518	2.885	1.294	0.863	0.588	0.818	0.059	69	1.938±0.262
	9→12	10.484	2.813	1.339	0.876	0.580	0.823	0.093	82	1.778±0.214
	12→15	13.552	2.738	1.386	0.887	0.665	0.853	0.136	53	1.132±0.169
	15→18	16.352	2.673	1.413	0.897	0.658	0.856	0.180	53	0.932±0.134
	18→21	19.311	2.580	1.451	0.909	0.773	0.895	0.231	41	0.861±0.141
	21→24	22.429	2.508	1.490	0.917	0.821	0.912	0.288	12	0.254±0.096
45→135	3→6	4.589	3.079	1.187	0.823	−0.546	0.080	0.031	60	2.525±0.366
	6→9	7.520	3.091	1.182	0.819	−0.513	−0.022	0.056	78	1.990±0.247
	9→12	10.456	3.073	1.194	0.821	−0.545	0.043	0.093	64	1.227±0.162
	12→15	13.456	3.070	1.193	0.823	−0.519	0.079	0.142	48	0.749±0.116
	15→18	16.412	3.207	1.091	0.789	−0.644	−0.157	0.212	21	0.449±0.100
135→225	3→6	4.462	3.183	1.119	0.798	0.373	−0.721	0.028	22	1.446±0.330
	6→9	7.392	3.277	1.074	0.772	0.438	−0.729	0.054	16	0.956±0.250
−135→−45	3→6	4.230	3.048	1.208	0.829	−0.480	0.159	0.030	17	3.551±1.011

TABLE III. The ratio R of the cross sections for the reactions $\gamma_V + d \rightarrow \pi^- + p + p_s$ and $\gamma_V + d \rightarrow \pi^+ + n + n_s$ derived from measurements with a deuterium target.

Bin		Kinematic averages				$(d\sigma/d\Omega)$ (μb/sr)		
ϕ (deg)	θ (deg)	θ (deg)	W (GeV)	Q^2 (GeV^2)	$-t$ (GeV^2)	$\pi^+ n$	$\pi^- p$	R
				(a) Data point 8 (D_2)				
all	0 → 3	1.840	2.138	1.212	0.073	5.242 ±0.700	3.174 ±0.422	0.605 ±0.114
−45 → 45	3 → 6	4.677	2.065	1.226	0.090	4.466 ±0.683	3.392 ±0.472	0.759 ±0.157
	6 → 9	7.583	2.022	1.234	0.110	4.662 ±0.574	2.290 ±0.319	0.626 ±0.103
	9 → 12	10.583	1.980	1.254	0.135	2.892 ±0.421	2.329 ±0.284	0.805 ±0.153
	12 → 15	13.225	1.942	1.275	0.161	1.979 ±0.321	1.510 ±0.212	0.763 ±0.164
	15 → 18	16.352	1.892	1.270	0.191	2.018 ±0.295	0.979 ±0.166	0.723 ±0.162
	18 → 21	19.391	1.852	1.307	0.234	1.941 ±0.330	1.347 ±0.221	0.694 ±0.164
	21 → 24	22.399	1.799	1.306	0.274	1.713 ±0.334	0.792 ±0.202	0.462 ±0.148
	24 → 27	25.414	1.746	1.308	0.315	1.175 ±0.302	0.672 ±0.184	0.512 ±0.215
	27 → 30	28.650	1.708	1.330	0.364	1.289 ±0.535	0.369 ±0.176	0.286 ±0.181
	30 → 33	31.424	1.669	1.352	0.404	1.977 ±0.690	0.748 ±0.282	0.378 ±0.195
45 → 135	3 → 6	4.566	2.143	1.200	0.078	3.590 ±0.596	2.975 ±0.372	0.829 ±0.160
	6 → 9	7.334	2.151	1.210	0.090	3.376 ±0.429	2.928 ±0.315	0.867 ±0.144
	9 → 12	10.519	2.159	1.190	0.107	2.740 ±0.347	2.110 ±0.241	0.770 ±0.131
	12 → 15	13.376	2.183	1.188	0.128	2.290 ±0.317	1.948 ±0.243	0.851 ±0.158
	15 → 18	16.135	2.211	1.175	0.153	1.669 ±0.306	1.448 ±0.238	0.868 ±0.214
	18 → 21	19.044	2.325	1.164	0.192	1.248 ±0.423	0.781 ±0.234	0.626 ±0.283
135 → 225	3 → 6	4.614	2.207	1.165	0.066	3.569 ±0.597	2.713 ±0.412	0.760 ±0.172
	6 → 9	7.526	2.256	1.151	0.073	3.058 ±0.448	2.745 ±0.346	0.898 ±0.173
	9 → 12	10.574	2.312	1.146	0.090	2.603 ±0.388	2.350 ±0.266	0.903 ±0.169
	12 → 15	13.361	2.363	1.120	0.113	2.297 ±0.329	1.432 ±0.193	0.623 ±0.123
	15 → 18	16.339	2.415	1.108	0.147	1.146 ±0.210	1.298 ±0.173	1.132 ±0.257
	18 → 21	19.620	2.471	1.082	0.197	1.036 ±0.192	0.720 ±0.125	0.695 ±0.177
	21 → 24	22.530	2.553	1.041	0.255	0.505 ±0.166	0.407 ±0.086	0.806 ±0.315
				(b) Data point 9 (D_2)				
all	0 → 3	1.982	3.063	1.187	0.020	2.804 ±0.383	1.988 ±0.298	0.709 ±0.144
−45 → 45	3 → 6	4.472	2.959	1.254	0.034	2.727 ±0.403	2.714 ±0.405	0.995 ±0.209
	6 → 9	7.518	2.885	1.294	0.059	1.938 ±0.262	1.824 ±0.252	0.941 ±0.182
	9 → 12	10.484	2.813	1.339	0.093	1.778 ±0.214	1.191 ±0.176	0.670 ±0.128
	12 → 15	13.552	2.738	1.386	0.136	1.131 ±0.169	0.755 ±0.132	0.668 ±0.154
	15 → 18	16.352	2.673	1.413	0.180	0.932 ±0.134	0.549 ±0.106	0.589 ±0.142
	18 → 21	19.311	2.580	1.451	0.231	0.861 ±0.141	0.426 ±0.095	0.495 ±0.137
	21 → 24	22.429	2.508	1.490	0.288	0.255 ±0.096	0.229 ±0.092	0.900 ±0.495
45 → 135	3 → 6	4.589	3.097	1.187	0.031	2.525 ±0.366	1.572 ±0.280	0.623 ±0.143
	6 → 9	7.520	3.091	1.182	0.056	1.990 ±0.247	1.291 ±0.185	0.649 ±0.123
	9 → 12	10.456	3.073	1.194	0.093	1.227 ±0.163	1.203 ±0.157	0.980 ±0.182
	12 → 15	13.456	3.070	1.193	0.142	0.749 ±0.116	0.696 ±0.117	0.929 ±0.212
	15 → 18	16.412	3.207	1.091	0.212	0.450 ±0.100	0.383 ±0.089	0.853 ±0.275
135 → 225	3 → 6	4.462	3.183	1.119	0.028	1.445 ±0.330	1.834 ±0.409	1.269 ±0.405
	6 → 9	7.392	3.277	1.074	0.054	0.956 ±0.250	1.212 ±0.289	1.268 ±0.448
				(c) Data point 13 (D_2)				
all	0 → 10		2.130		0.469	0.393 ±0.066	0.173 ±0.042	0.440 ±0.129

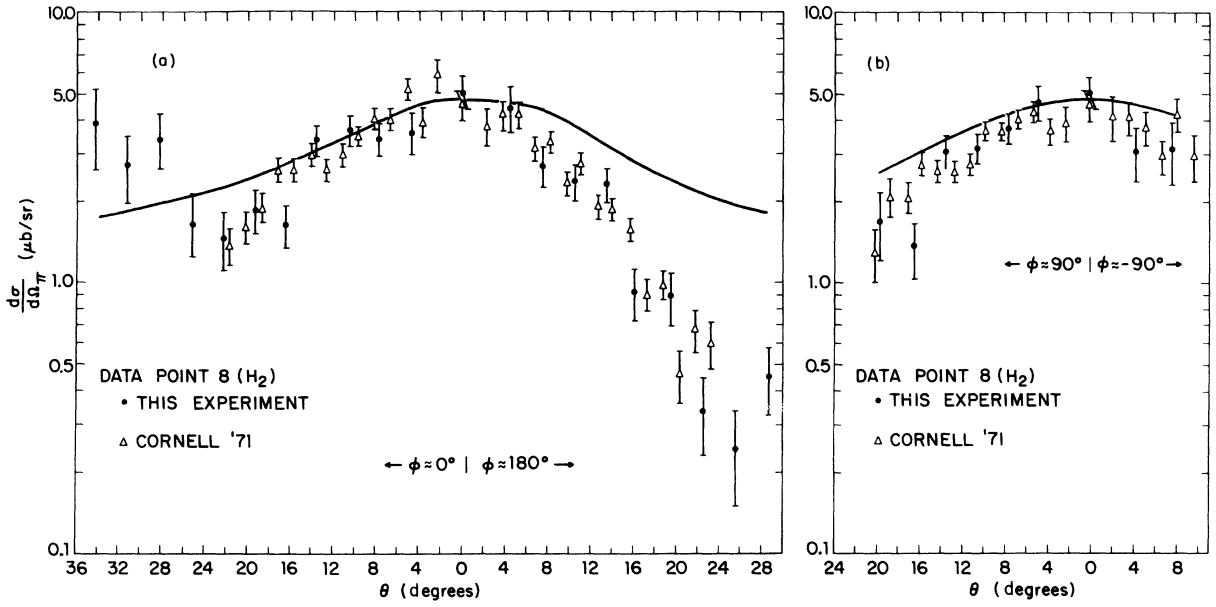

FIG. 5. A plot of the virtual-photoproduction cross section versus θ for data point 8 together with the cross section for the similar point determined in an earlier experiment at Cornell. For this data point $W = 2.15$ GeV, $Q^2 = 1.2$ GeV^2. The solid curves are the predictions of Berends's theory with the empirical addition of the isoscalar component.

encountered in the analysis of this experiment is 4%. This will produce roughly a 2% error in the pion form factor.

Table IV summarizes the isovector components of the cross section and the calculated values of the pion form factor using the measured value of R and assuming that $R = 1$. Table V summarizes the values of the pion form factor calculated from previously reported cross sections using values of R determined in this experiment. The errors in the pion form factor are statistical only and do not include the estimated over-all error in normalization. The correction for the isoscalar component changes the pion form factor by less than 10% at all points except the highest Q^2 point. At the $Q^2 = 4$ GeV^2 point, the correction for the isoscalar component decreases F by 20%. Figure 15 shows the variation with Q^2 of the pion form factor.

The single pole expression

$$F = \frac{1}{1 + Q^2/m_V^2}$$

gives a good fit to the data with

$$m_V^2 = (0.471 \pm 0.010)\ \text{GeV}^2 .$$

The χ^2 is 20.4 with 16 degrees of freedom. This fit gives for the electromagnetic radius of the pion

$$\langle r_\pi^2 \rangle^{1/2} = (0.704 \pm 0.007)\ \text{fm}.$$

The uncertainty in the mass parameter, m_V^2, and the pion radius due to the estimated 7% uncertainty in the over-all normalization can be estimated by fitting the data to the expression

$$F = \frac{N}{1 + Q^2/m_V^2},$$

with the assumption of an additional data point at $Q^2 = 0$ with the value 1 ± 0.04. Such a fit gives

$$N = 1.029 \pm 0.035,$$

$$m_V^2 = (0.451 \pm 0.025)\ \text{GeV}^2,$$

$$\langle r_\pi^2 \rangle^{1/2} = (0.730 \pm 0.024)\ \text{fm}.$$

The χ^2 is 19.5 with 16 degrees of freedom.

This value for the pion form factor is in agreement with the value

$$\langle r_\pi^2 \rangle^{1/2} = (0.78 \pm 0.09)\ \text{fm}$$

reported by the Dubna-Serpukhov-UCLA collaboration from a direct measurement of pion electron scattering.[24] It also agrees with a study of the inverse electroproduction reaction $\pi^- p \to e^+ e^- n$ carried out by a Dubna group.[25] They obtained

$$\langle r_\pi^2 \rangle^{1/2} = (0.73 \pm 0.13)\ \text{fm}.$$

A more general discussion including the analysis of colliding-beam experiments is given by Gourdin.[4]

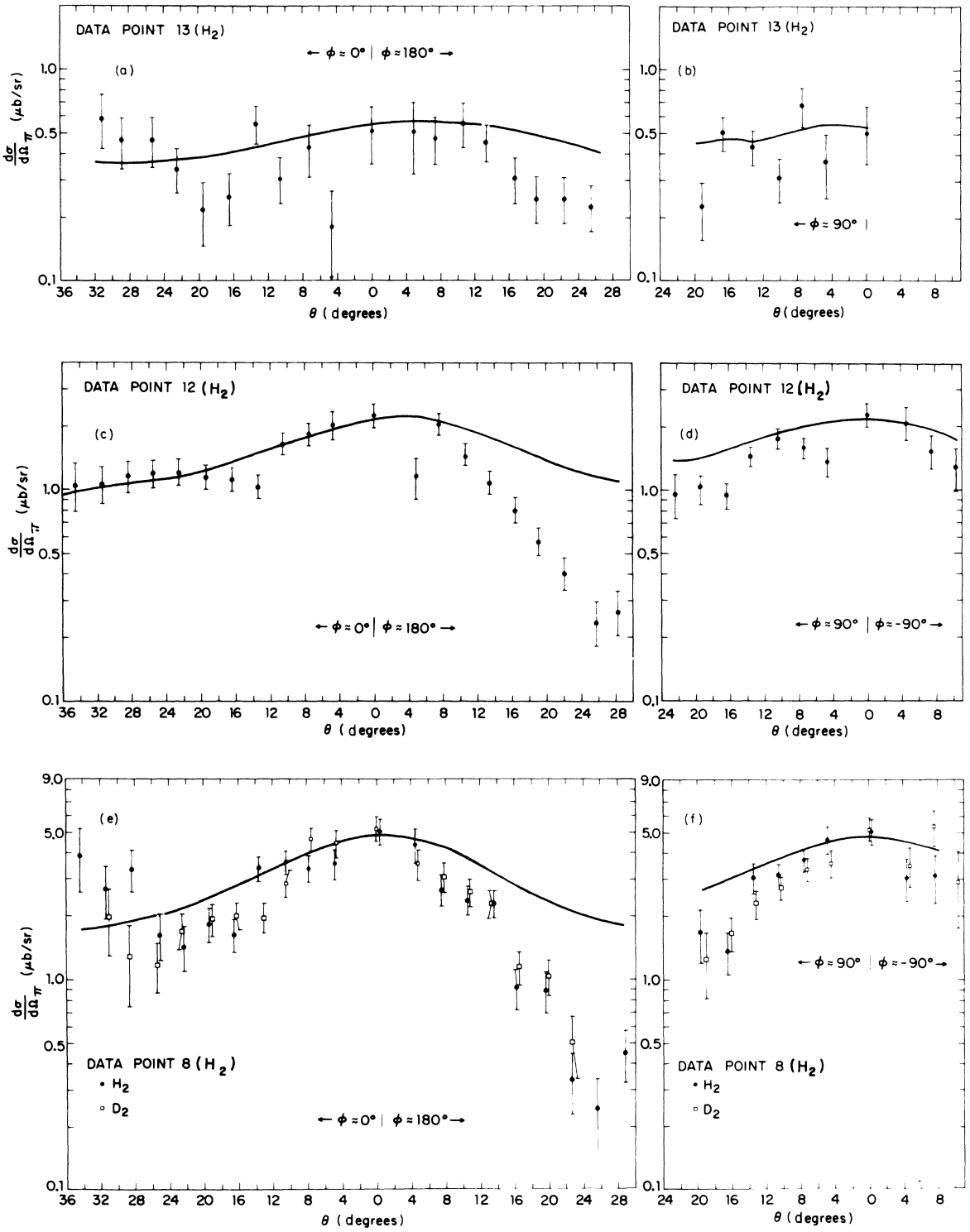

FIG. 6. A plot of the virtual-photoproduction cross sections for the $\pi^+ n$ reaction versus θ for data points 8, 12, and 13. These points have $W = 2.15$ GeV^2 and different Q^2. The graph for point 8 shows the data from both the hydrogen and deuterium targets. The solid curves are the prediction of Berends's theory with the empirical addition of the isoscalar component. For point 8, $W = 2.15$ GeV, $Q^2 = 1.2$ GeV^2; for point 12, $W = 2.15$ GeV, $Q^2 = 2.0$ GeV^2; for point 13, $W = 2.15$ GeV, $Q^2 = 4.0$ GeV^2.

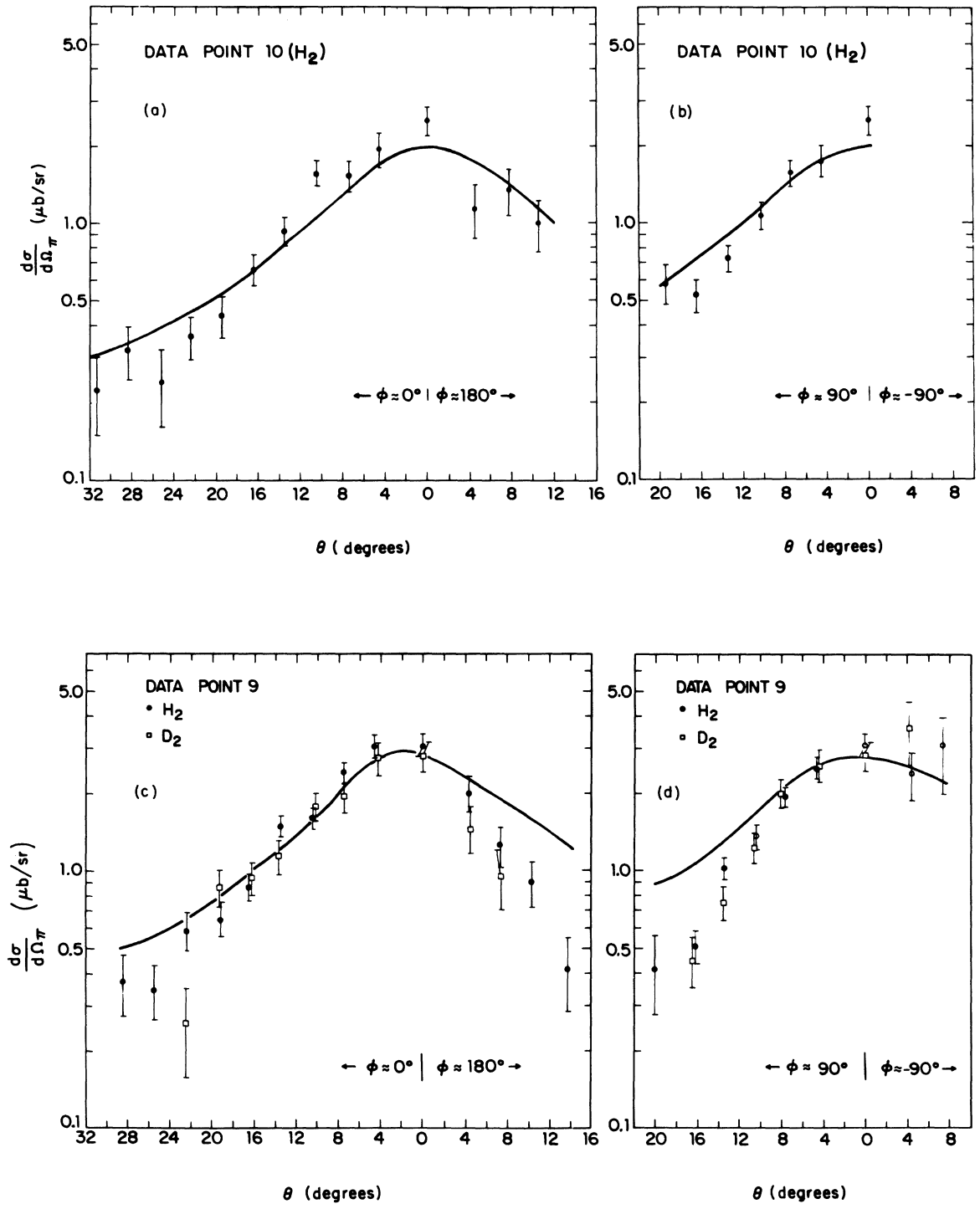

FIG. 7. A plot of the virtual-photoproduction cross section for the $\pi^+ n$ reaction versus θ for data points 9 and 10. These points have $W = 3.11$ GeV, $Q^2 = 1.2$ GeV^2, and 1.7 GeV^2, respectively. The graph for point 9 shows the data from both the hydrogen and deuterium targets. The solid curves are the predictions of Berends's theory with the empirical addition of the isoscalar component.

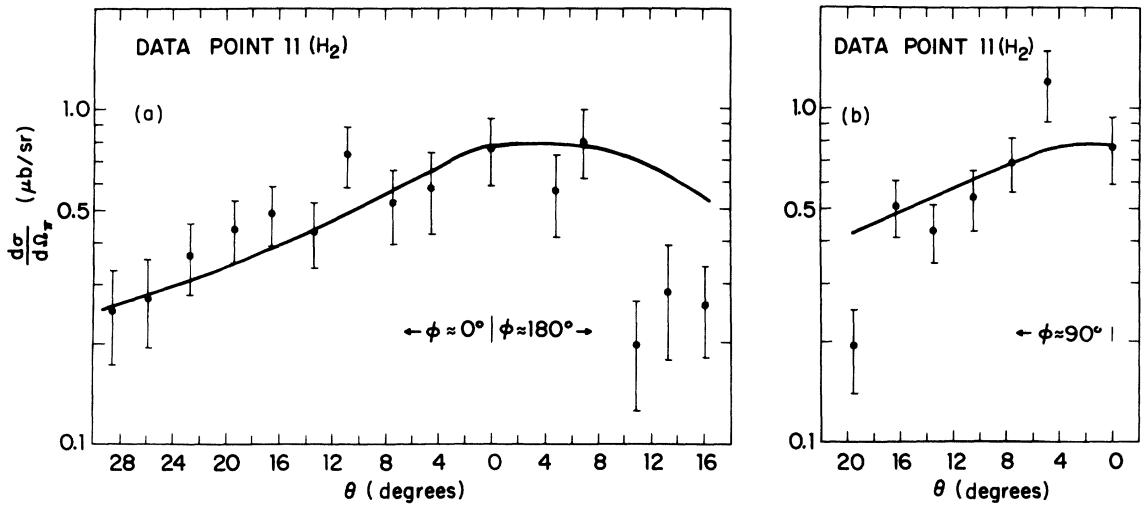

FIG. 8. A plot of the virtual-photoproduction cross section for the $\pi^+ n$ reaction versus θ for data point 11. For this data point $W = 2.67$ GeV, $Q^2 = 3.41$ GeV^2. The solid curves are the predictions of Berends's theory with the empirical addition of the isoscalar component.

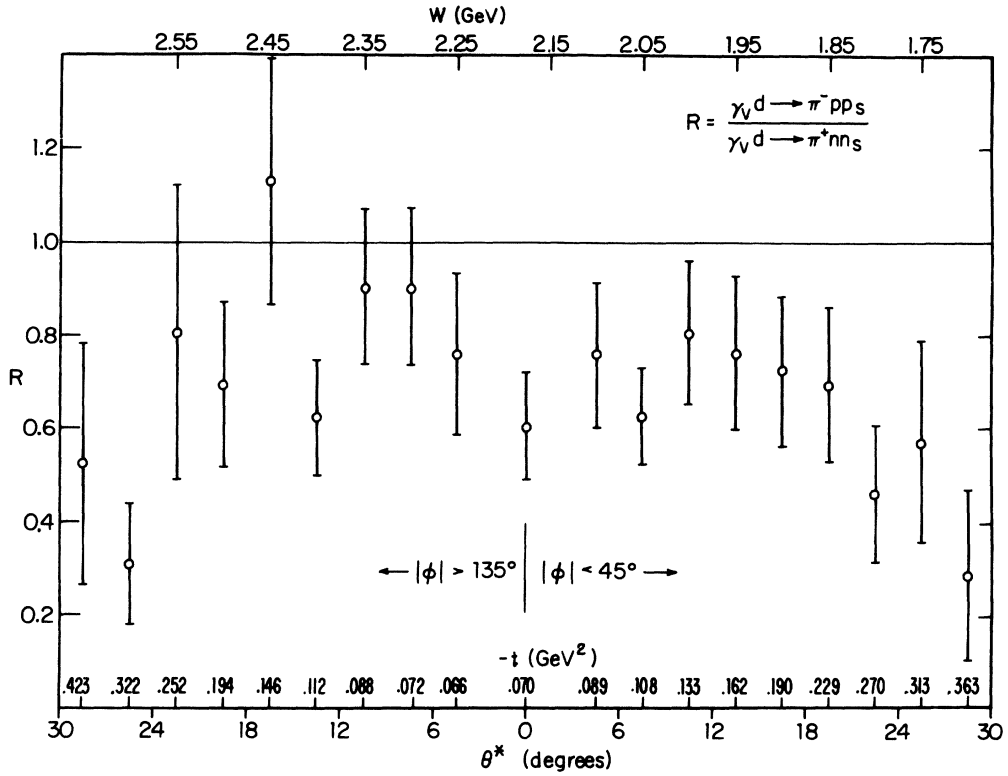

FIG. 9. The measured ratio R of the cross sections for the production of single π^- and π^+ mesons from deuterium at data point 8 where the nominal values are $W = 2.15$ GeV, $Q^2 = 1.2$ GeV^2. The lower scale shows the momentum transfer and the πN center-of-mass production angle. The upper scale shows the total πN center-of-mass energy. For these data the production plane is dominantly parallel to the electron-scattering plane.

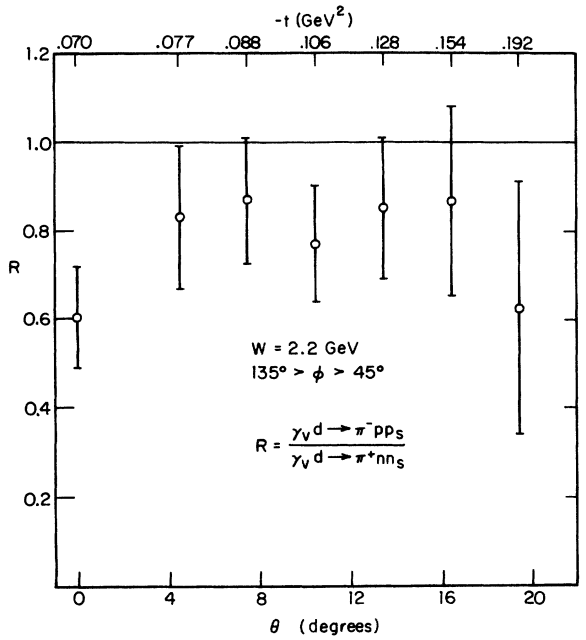

FIG. 10. The measured ratio R of the cross sections for the production of single π^- and π^+ mesons from deuterium at data point 8 where the nominal values are $W = 2.15$ GeV, $Q^2 = 1.2$ GeV^2. For these data the production plane is dominantly perpendicular to the electron-scattering plane. The upper scale shows the momentum transfer, the lower scale the center-of-mass production angle. W does not vary for these data.

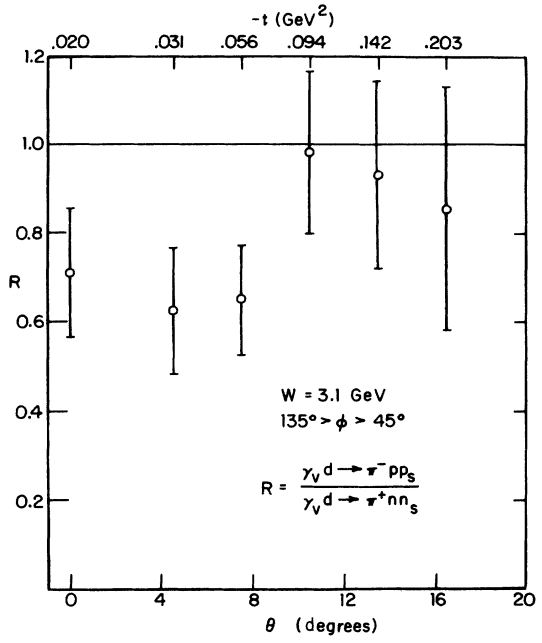

FIG. 12. The measured ratio of the cross sections for the production of single π^- and π^+ mesons from deuterium at data point 8 where the nominal values are $W = 3.11$ GeV, $Q^2 = 1.2$ GeV^2. For these data the production plane is dominantly perpendicular to the electron-scattering plane. The upper scale shows the momentum transfer, the lower scale the center-of-mass production angle. W does not vary appreciably for these data.

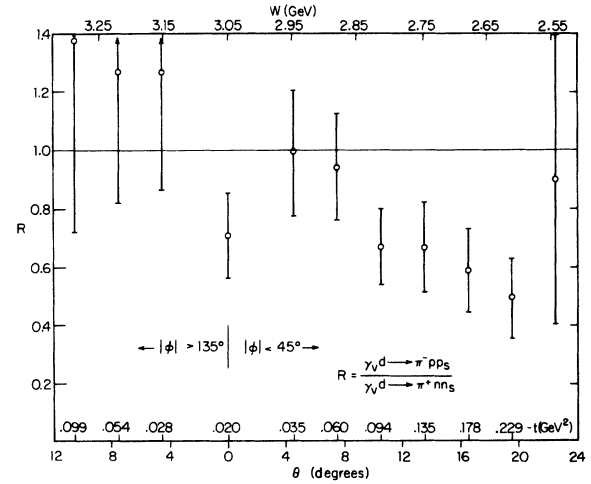

FIG. 11. The measured ratio R of the cross sections for the production of single π^- and π^+ mesons from deuterium at data point 9 where the nominal values are $W = 3.11$ GeV, $Q^2 = 1.2$ GeV^2. The lower scale gives the momentum transfer and the πN center-of-mass production angle. The upper scale gives the total πN center-of-mass energy. For these data the production plane is dominantly coincident with the electron-scattering plane.

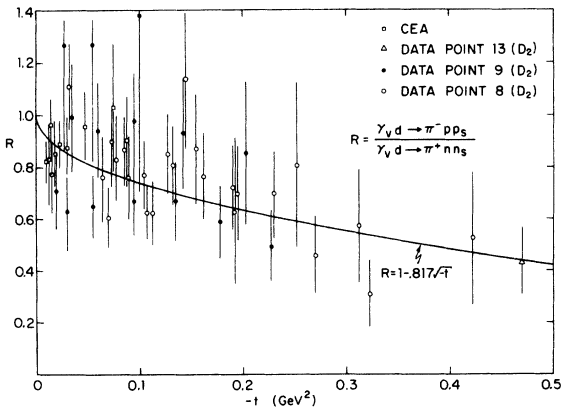

FIG. 13. A plot of R versus momentum transfer for the data from this experiment and the earlier CEA experiment together with a fit of the form $(1 - A\sqrt{-t})$.

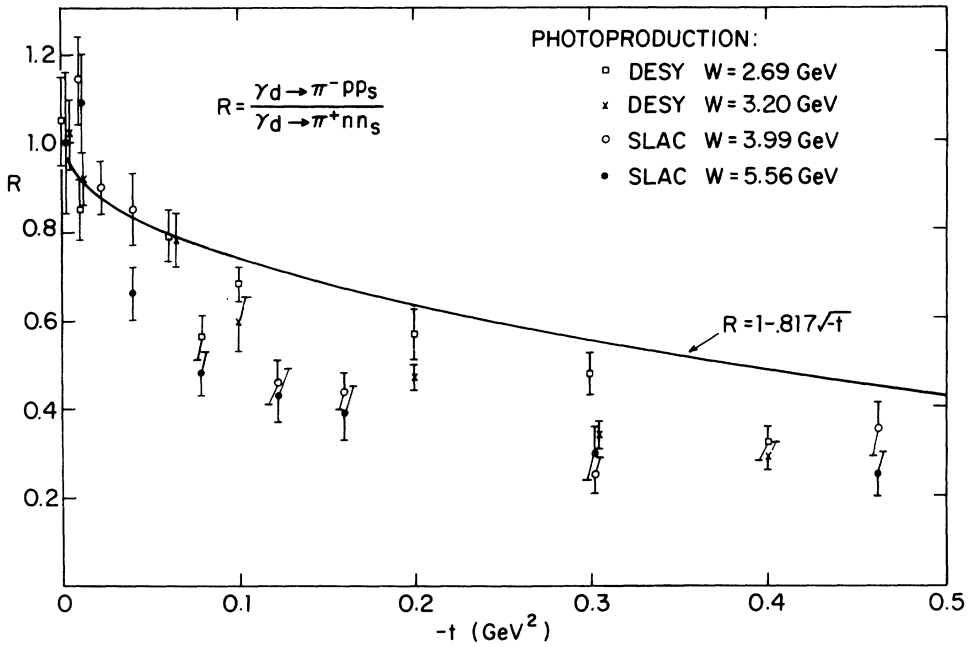

FIG. 14. A plot of R versus $\sqrt{-t}$ for photoproduction data. The solid line is the fit to the electroproduction data determined from the measurements reported in this experiment.

V. DISCUSSION

In addition to using the forward cross section to determine the pion form factor it is instructive to examine the validity of the theory over a wider angular range. The solid curves in Figs. 5 through 8 show the predictions of Berends's theory calculated using as input the measured pion form factor and the measured value for R. As has been observed previously the theory does not predict correctly the scalar-transverse interference, the transverse-transverse interference term, or the t dependence at large t.

We now have sufficient data to see if the theory gives the same value for the pion form factor at data points with the same Q^2 and different W. These points differ in that the minimum momentum transfer decreases as W increases. Figure 16 summarizes the pion form factor found for the different points at $Q^2 = 1.2$ GeV^2 and 2.0 GeV^2. The agreement of the values for the pion form factor obtained at the same Q^2 shows that there is no dependence on the minimum momentum transfer. The agreement is even better if one corrects for a possible difference in normalization of the different experiments by dividing the form factors

TABLE IV. The values of the pion form factor determined from this experiment using the data for $\theta \leq 3°$. The uncorrected columns refer to the raw cross section and the pion form factor determined from it. The isovector columns give the calculated isovector component and the pion form factor determined from it. Uncertainties are statistical only.

			Uncorrected			Isovector	
Data point	Q^2 (GeV^2)	$\langle -t \rangle$ (GeV^2)	$(d\sigma/d\Omega)$ (μb/sr)	F_π	R	$(d\sigma/d\Omega)$ (μb/sr)	F_π
8	1.216	0.069	5.077 ±0.740	0.324 ±0.028	0.786	4.534 ±0.661	0.292 ±0.026
9	1.198	0.019	3.089 ±0.309	0.321 ±0.018	0.888	2.916 ±0.292	0.305 ±0.017
10	1.712	0.034	2.517 ±0.325	0.257 ±0.018	0.850	2.328 ±0.301	0.246 ±0.017
11	3.301	0.162	0.769 ±0.174	0.136 ±0.017	0.672	0.643 ±0.145	0.123 ±0.015
12	1.988	0.157	2.280 ±0.289	0.221 ±0.016	0.676	1.911 ±0.242	0.199 ±0.015
13	3.991	0.477	0.512 ±0.156	0.124 ±0.022	0.436	0.368 ±0.112	0.101 ±0.019

TABLE V. The values of the pion form factor determined from cross sections for $\theta \leq 3°$ reported in earlier CEA (see Ref. 1) and Cornell (see Ref. 3) experiments. The uncorrected columns refer to the raw cross section and the pion form factor determined from it. The isovector columns give the calculated isovector component and the pion form factor calculated from it. Uncertainties are statistical only.

			Uncorrected			Isovector	
Data point	Q^2 (GeV^2)	$\langle -t \rangle$ (GeV^2)	$(d\sigma/d\Omega)$ (μb/sr)	F_π	R	$(d\sigma/d\Omega)$ (μb/sr)	F_π
			(a) CEA data				
4	0.176	0.003	7.15 ± 0.34	0.810 ± 0.044	0.952	6.99 ± 0.33	0.786 ± 0.045
3b	0.294	0.006	8.05 ± 0.44	0.641 ± 0.028	0.936	7.79 ± 0.43	0.606 ± 0.028
7	0.396	0.011	8.90 ± 0.34	0.577 ± 0.016	0.914	8.52 ± 0.33	0.550 ± 0.015
9	0.795	0.034	6.99 ± 0.37	0.400 ± 0.013	0.850	6.47 ± 0.34	0.380 ± 0.013
12	1.188	0.066	3.54 ± 0.28	0.276 ± 0.014	0.790	3.16 ± 0.25	0.256 ± 0.013
			(b) Cornell '71 data				
1	0.620	0.011	5.15 ± 0.25	0.465 ± 0.015	0.914	4.93 ± 0.24	0.453 ± 0.014
2	1.069	0.019	3.53 ± 0.31	0.323 ± 0.017	0.888	3.33 ± 0.29	0.321 ± 0.017
3	1.204	0.031	3.61 ± 0.23	0.291 ± 0.010	0.856	3.35 ± 0.21	0.279 ± 0.010
4	1.314	0.048	3.50 ± 0.29	0.266 ± 0.013	0.822	3.19 ± 0.27	0.252 ± 0.012
6	1.200	0.069	4.43 ± 0.29	0.288 ± 0.012	0.786	3.95 ± 0.26	0.269 ± 0.011
7	2.015	0.070	1.59 ± 0.17	0.185 ± 0.011	0.784	1.42 ± 0.15	0.174 ± 0.010

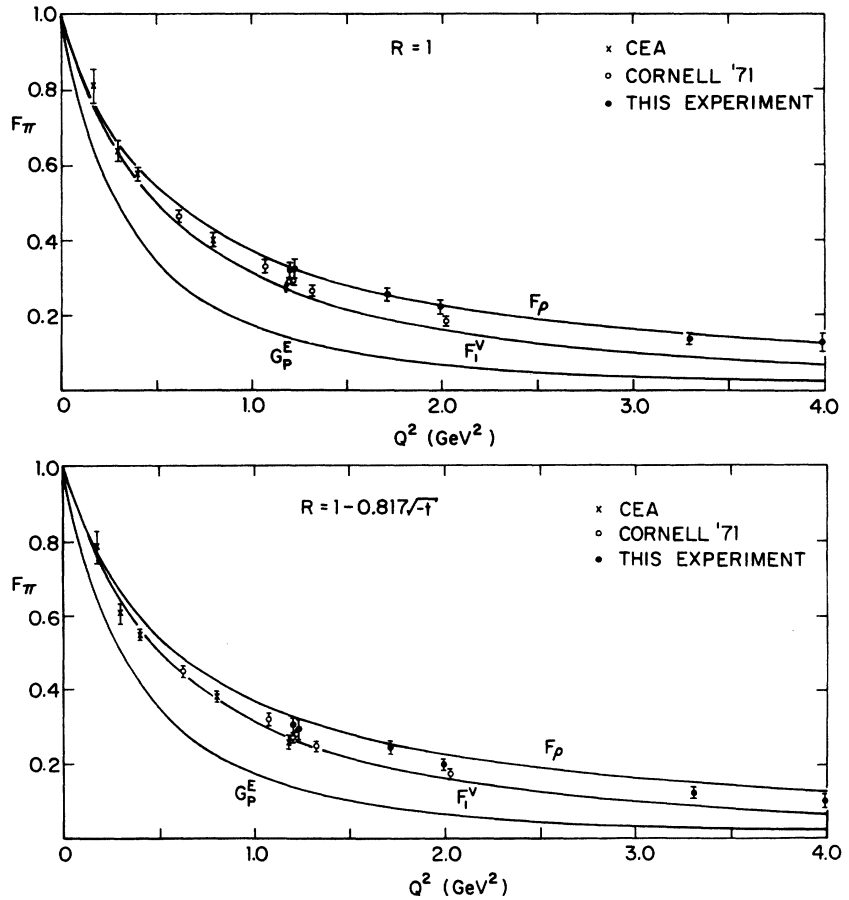

FIG. 15. The values for the pion electromagnetic form factor derived from the data reported in this and earlier experiments using the dispersion theory of Berends: (a) for no isoscalar component and (b) for an isoscalar component given by $R = 1 - 0.817\sqrt{-t}$. The CEA data are taken from Ref. 1; the Cornell '71 data from Ref. 3.

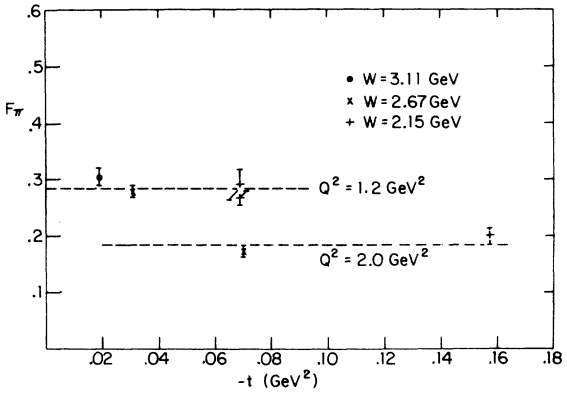

FIG. 16. A plot showing the dependence of the value of the pion form factor on the minimum momentum transfer. All of the high points were from this experiment; the low points were from the Cornell '71 experiment.

by the form factor determined at the common data point $W = 2.15$ GeV, $Q^2 = 1.2$ GeV^2.

The increase in the isoscalar component with Q^2 at fixed W is quite interesting and has no explanation within the context of the present theory. The isoscalar component observed in photoproduction is explained by the introduction of additional t-channel contributions such as ρ, B, and A_2 exchange.[22,23,26] In view of the increasing dominance of the one-pion exchange term at high Q^2, this suggests that diagrams such as that shown in Fig. 17 give an increasingly important contribution to the cross section. It will be instructive to have available a longitudinal-transverse separation so that one can further ascertain the character of these additional diagrams.

Questions have been raised as to the validity of using this technique to determine the pion form factor. Dombey and Read[27] pointed out that the PCAC (partial conservation of axial-vector current) low-energy theorems giving the dependence of the charged pion electroproduction amplitude on the axial-vector form factor are inconsistent with the dispersion theoretic calculations in which the axial-vector form factor played no role. The basic reason is that the Born approximation terms taken from the pseudoscalar theory of the pion-nucleon coupling do not satisfy PCAC requirements. They further pointed out that the Born approximation terms chosen from pseudovector theory satisfy PCAC but introduce ambiguity into the determination of the pion form factor through the unknown character of the axial-vector form factor. This point remains unresolved in the literature and further theoretical work is required to reconcile PCAC requirements with the more conventional extrapolation from electroproduction.

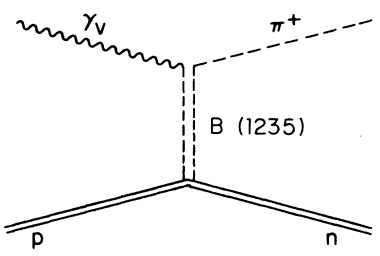

FIG. 17. An additional diagram that could contribute to the isoscalar component of the cross section.

Kellett and Verzegnassi[28] questioned the treatment of one of the subtraction constants in the Born approximation treatments of Berends[2] and Devenish and Lyth.[29] They pointed out that a subtraction constant that might be required for one particular term could be a function of t and Q^2 and thus introduce ambiguity into the determination of the pion form factor. They stressed the importance of measurements with fixed k^2 at different t as a means for determining this unknown function. In electroproduction the best way to make such measurements is to vary W and keep Q^2 fixed. This provides a set of data with the same k^2 and different t at 0° where the theory should work best. Figure 16 shows such data for $Q^2 = 1.2$ and 2.0 GeV^2. The measured form factor depends on Q^2 and not $t_{\min}$. This indicates that the Kellett-Verzengnassi subtraction constant is not important and that Berends was correct in using an unsubtracted dispersion relationship.

More recently Actor, Körner, and Bender[30] have extrapolated an explicitly dual model for pion photoproduction to electroproduction. They are led to an essentially unique electroproduction ansatz which fits the DESY data. This model behaves qualitatively like an electric Born term model with a flat nucleon form factor and a vector dominance pion form factor. This suggests that the determination of the pion form factor is not particularly sensitive to the form of the theory used to extrapolate from photoproduction to electroproduction.

The best way to settle the argument concerning the determination of the pion form factor is to make a direct extrapolation to the pion pole. It is clear from the work of Devenish and Lyth[29] that such a procedure will work if one has sufficiently precise and detailed data. It is within the realm of present techniques to obtain data of the prerequisite quantity and precision.

The theoretical calculations shown in Fig. 1 indicate that, for modest Q^2, as the energy increases the cross section does not decrease. This behavior is due to the increasing dominance of one-pion

exchange; it suggests that single-pion electroproduction will continue to be a significant part of the total virtual-photoproduction cross section even at very high energies.

ACKNOWLEDGMENTS

We would like to thank the Director, Professor Boyce McDaniel, and the staff of the Wilson Synchrotron Laboratory for their help during the course of this experiment. We would like to thank the ES group for the loan of their spectrometer. We also thank the staff of the Harvard Cyclotron Laboratory for assistance in the construction of the apparatus. The program for the electric-Born-model prediction was obtained from Professor F. Berends.

---

*Present address: Fermi National Accelerator Laboratory, P. O. Box 500, Batavia, Illinois 60510.

‡Present address: P. O. Box 29246, Los Angeles, Calif. 90029.

§Present address: 36 Webb St., Lexington, Mass. 02173.

†Research supported in part by U. S. Atomic Energy Commission Contract No. AT(11-1)-3064.

[1]For a brief summary of the theory and a more complete set of references see C. N. Brown, C. R. Canizares, W. E. Cooper, A. M. Eisner, G. J. Feldman, C. A. Lichtenstein, L. Litt, W. Lockeretz, V. B. Montana, and F. M. Pipkin, Phys. Rev. D 8, 92 (1973).

[2]The calculation used the dispersion theory formulation of F. A. Berends. For a description see Phys. Rev. D 1, 2590 (1970).

[3]C. J. Bebek, C. N. Brown, M. Herzlinger, S. Holmes, C. A. Lichtenstein, F. M. Pipkin, L. K. Sisterson, D. Andrews, K. Berkelman, D. G. Cassel, and D. L. Hartill, Phys. Rev. D 9, 1229 (1974).

[4]For a general review of our present theoretical understanding of the pion form factor see M. Gourdin, Phys. Rep. 11C, 29 (1974).

[5]C. Driver, K. Heinloth, K. Höhne, G. Hofmann, P. Karow, D. Schmidt, G. Specht, and J. Rathje, Phys. Lett. 35B, 77 (1971).

[6]P. S. Kummer, A. B. Clegg, F. Foster, G. Hughes, R. Siddle, J. Allison, B. Dickinson, E. Evangelides, M. Ibbotson, R. Lawson, R. S. Meaburn, H. E. Montgomery, W. J. Shuttleworth, and A. Sofair, Nuovo Cimento Lett. 1, 1026 (1971).

[7]A. Sofair, J. Allison, B. Dickinson, E. Evangelides, M. Ibbotson, R. Lawson, R. S. Meaburn, H. E. Montgomery, W. J. Shuttleworth, A. B. Clegg, F. Foster, G. Hughes, P. Kummer, and R. Siddle, Nucl. Phys. B42, 369 (1972).

[8]C. R. Canizares, Ph.D. thesis submitted to Harvard University, 1971 (unpublished).

[9]A. Bartl and P. Urban, Acta. Phys. Austriaca 24, 139 (1966).

[10]N. Meister and D. R. Yennie, Phys. Rev. 130, 1210 (1963).

[11]P. Heide, U. Kötz, R. A. Lewis, P. Schmüser, H. J. Skronn, and H. Wahl, Phys. Rev. Lett. 21, 248 (1968).

[12]A. M. Boyarski, R. Diebold, S. D. Ecklund, G. F. Fischer, Y. Murata, B. Richter, and W. S. C. Williams, Phys. Rev. Lett. 21, 1767 (1968).

[13]P. E. Scheffler and P. L. Walden, Nucl. Phys. B75, 125 (1974).

[14]G. F. Chew and H. W. Lewis, Phys. Rev. 84, 779 (1951).

[15]A. Dar and A. Gal, Phys. Rev. Lett. 21, 444 (1968).

[16]K. Schilling, Nucl. Phys. B7, 498 (1968).

[17]A. Dar and A. Gal, Phys. Rev. D 1, 2714 (1970).

[18]D. I. Julius, Nucl. Phys. B27, 269 (1971).

[19]V. Franco and R. J. Glauber, Phys. Rev. 142, 1195 (1966); R. J. Glauber and V. Franco, *ibid.* 156, 1685 (1967).

[20]C. N. Brown, C. R. Canizares, W. E. Cooper, A. M. Eisner, G. J. Feldman, C. A. Lichtenstein, L. Litt, W. Lockeretz, V. B. Montana, and F. M. Pipkin, Phys. Rev. Lett. 27, 536 (1971).

[21]Z. Bar-Yam, J. de Pagter, M. M. Hoenig, W. Kern, D. Luckey, and L. S. Osborne, Phys. Rev. Lett. 19, 40 (1967).

[22]R. Worden, Nucl. Phys. B37, 253 (1972).

[23]G. Goldstein and J. F. Owens III (unpublished).

[24]G. T. Adylov, F. K. Aliev, D. Yu. Bardin, W. Gajewski, I. Ion, B. A. Kulakov, G. V. Micelmacher, B. Niczyporuk, T. S. Nigmanov, E. N. Tsyganov, M. Turala, A. S. Vodopianov, K. Wala, E. Dally, D. Drickey, A. Liberman, P. Shepard, J. Tompkins, C. Buchanan, and J. Poirier, Phys. Lett. 51B, 402 (1974).

[25]S. F. Berezhnev, L. S. Vertogradov, A. V. Dem'yanov, A. V. Kulikov, A. V. Kuptsov, G. C. Mkrtchyan, L. L. Nemenov, G. I. Smirnov, D. M. Khazins, and Yu. M. Chirkin, Yad. Fiz. 16, 185 (1972) [Sov. J. Nucl. Phys. 16, 99 (1973)].

[26]R. Diebold, Phys. Rev. Lett. 22, 204 (1969).

[27]N. Dombey and B. J. Read, Nucl. Phys. B60, 65 (1973).

[28]B. H. Kellett and C. Verzegnassi, Nuovo Cimento 13A, 195 (1973).

[29]R. C. E. Devenish and D. H. Lyth, Phys. Rev. D 5, 47 (1972).

[30]A. Actor, J. G. Körner, and I. Bender, Nuovo Cimento 24A, 369 (1974).